J|A|C|S COMMUNICATIONS

Published on Web 07/06/2010

Kinetics of Amyloid β Monomer-to-Oligomer Exchange by NMR Relaxation

Nicolas L. Fawzi, Jinfa Ying, Dennis A. Torchia, and G. Marius Clore*

Laboratory of Chemical Physics, National Institute of Diabetes and Digestive and Kidney Diseases, National Institutes of Health, Bethesda, Maryland 20892-0520

Received June 2, 2010; E-mail: mariusc@mail.nih.gov

Abstract: Recent studies have implicated non-fibrillar oligomers of the amyloid β (Aβ) peptide as the primary toxic species in Alzheimer's disease. Detailed structural and kinetic characterization of these states, however, has been difficult. Here we use NMR relaxation measurements to address the kinetics of exchange between monomeric and large, polymorphic oligomeric species of Aβ(1−40). ^{15}N and $^{1}H_N$ R_2 data at multiple magnetic fields were recorded for several peptide concentrations subsequent to the establishment of a stable pseudo-equilibrium between monomeric and NMR-invisible soluble oligomeric species. The increase in ^{15}N and $^{1}H_N$ R_2 rates as a function of protein concentration is independent of nucleus and magnetic field and shows only a small degree of variation along the peptide chain. This phenomenon is due to a lifetime broadening effect arising from the unidirectional conversion of monomer to the NMR-invisible oligomeric species ("dark" state). At a total Aβ(1−40) concentration of 300 μM, the apparent first-order rate constant for this process is $\sim$3 s^{-1}. Fitting the McConnell equations for two dipolar-coupled spins in two-site exchange to transfer-of-saturation profiles at two radiofrequency field strengths gives an estimate for k_{off} of 73 s^{-1} and transiently bound monomer $^{1}H_N$ R_2 rates of up to 42 000 s^{-1} in the tightly bound central hydrophobic region and $\sim$300 s^{-1} in the disordered regions, such as the first nine residues. The fraction of peptide within the "dark" oligomeric state undergoing exchange with free monomer is calculated to be $\sim$3%.

Alzheimer's disease (AD) is characterized by plaques of amyloid β (Aβ) fibrils.[1] The link, however, between the fibrils and the etiology of the disease is not well understood.[2] Recent evidence suggests that smaller, less ordered oligomers of Aβ (ranging from 40 to 200 kDa) may be primarily responsible for neurotoxicity,[3] and their presence in cerebrospinal fluid correlates with AD.[4] Elucidating the mechanism of conversion of non-toxic monomers to toxic oligomers or fibrils may be critical to the design of therapeutic interventions that steer the equilibrium away from the buildup of toxic species.[5] While Aβ fibrils have been studied at the atomic level by fiber diffraction,[6] solid-state NMR,[7] electron microscopy (EM),[8] and H/D exchange combined with mutagenesis,[9] characterization of the non-fibrillar oligomeric states has proven difficult due to their heterogeneous nature.[5] Recent work has provided some information on Aβ oligomers,[10] but the chemical cross-linking reagents, ionization conditions, organic solvents, and detergents used in these studies make comparison with oligomers formed in their absence difficult.[5,11] Several fundamental questions concerning the nature of Aβ oligomers remain to be answered, including whether the oligomers are permanently stable or if they are constantly forming from and dissociating back into monomers in a dynamic equilibrium preceding the formation of the extremely stable amyloid fibrils.[12] In this study, we make use of solution NMR relaxation measurements to directly observe rapid exchange under pseudo-equilibrium conditions between monomeric Aβ peptide and non-fibrillar oligomers formed spontaneously in a standard buffer without organic solvents or detergents. These data provide significant details concerning the pre-fibrillar equilibrium that are difficult to probe by other biophysical techniques.

Samples of uniformly ^{15}N-labeled Aβ(1−40) peptide were prepared from NaOH-treated stocks to remove fibril seeds.[13] NMR samples comprised 60, 150, and 300 μM Aβ(1−40) in 50 mM HEPES, pH 6.8, and 90% H_2O/10% D_2O. All solutions were prefiltered in the presence of the chelating agent Chelex 100 (Sigma-Aldrich) to remove any potential trace metal contamination.[14] Samples were prepared and maintained between 4 and 10 °C, and all NMR experiments were conducted at 10 °C. Under these conditions, Aβ(1−40) at a concentration of 60 μM remains stable for many weeks, as monitored by following the $^{1}H_N$/^{15}N cross-peak intensities in ^{1}H−^{15}N HSQC correlation spectra (Figures 1A,B) over time. At peptide concentrations of 150 and 300 μM, however, the signal intensities decay uniformly across the peptide over a period of about 1 week, after which a pseudo-equilibrium is established with integrated intensities for the backbone amide ($^{1}H_N$) envelope (measured from the first t_1 increment of an HSQC spectrum) of 70 and 40% of their original values, corresponding to monomer concentrations of 105 and 130 μM, respectively (Figure 1B). Since the $^{1}H_N$/^{15}N observed cross-peaks arise solely from monomeric peptide[13,15,16] and no new cross-peaks appear, the decrease in signal intensity must arise from the conversion of monomer to a species whose NMR signals are broadened beyond detection due to large oligomer size and correspondingly long rotational correlation times. These large species remain in solution, as the samples are clear. Once equilibrated, the presence of large polydisperse aggregates was confirmed by dynamic light scattering, and transmision EM revealed the presence of elongated, morphologically disordered non-fibrillar aggregates with possibly some small, needle-like fibrils present (Figure 2), similar to those observed for other proteins.[17]

^{15}N and $^{1}H_N$ transverse relaxation (R_2) rates (Figure 1C) were measured for the equilibrated Aβ(1−40) samples using 2D ^{1}H−^{15}N HSQC-based experiments.[14,18] The R_2 rates increase as a function of total peptide concentration (Figure 3). The difference in R_2 rates, ΔR_2, between high (150 or 300 μM) and low (60 μM) concentration samples is independent of nucleus or magnetic field (Figure 3B,C), as evidenced by the linear ΔR_2 correlation plots with a slope of $\sim$1 (Figure 4). In addition, the variation in ΔR_2 across the peptide chain is small, with average ΔR_2(150 − 60 μM) and ΔR_2(300 − 60 μM) values of 0.7 ± 0.3 and 2.4 ± 0.5 s^{-1}, respectively. The ΔR_2 values are slightly higher for the hydrophobic (green lettering) segments spanning Leu17 to Ala21 and Ala30 to Val40, with the former being systematically elevated relative to the latter. These two regions correspond to the exterior and interior in-register parallel β-strands, respectively, of the cross-β core of Aβ(1−40) amyloid fibrils.[7a,b]

 10.1021/ja1048253

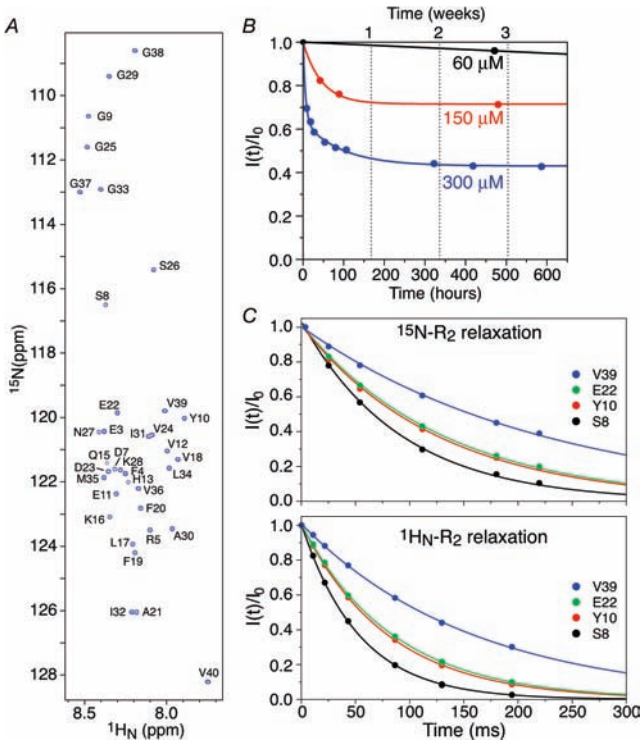

Figure 1. (A) 900 MHz $^{1}H-^{15}N$ HSQC correlation spectrum of 60 μM Aβ(1−40) at 10 °C. (B) Time dependence of the integrated intensity of the $^{1}H_N$ envelope (measured from the first t_1 increment of a $^{1}H-^{15}N$ HSQC spectrum) for 60 (black), 150 (red), and 300 (blue) μM Aβ(1−40) samples. The solid lines represent single- or double-exponential fits to the 150 or 300 μM Aβ(1−40) data, respectively. The double-exponential fitting function is given by $I(t)/I_0 = A_1\, e^{-t/\tau_1} + A_2\, e^{-t/\tau_2} + (1 - A_1 - A_2)$, where τ_1 and τ_2 are characteristic time constants, and A_1 and A_2 are the associated amplitudes. The parameter A_2 is set to 0 for the single-exponential fit. For the 150 μM sample, $\tau_1 = 51$ h and $A_1 = 0.31$; for the 300 μM sample, $\tau_1 = 6$ h, $\tau_2 = 93$ h, $A_1 = 0.36$, and $A_2 = 0.21$. At both 150 and 300 μM total concentrations, the samples reach pseudo-equilibrium after about 100 h, after which the signal intensity does not change more than a few percent on the time scale of a complete NMR experiment (4−12 h). (C) ^{15}N (top) and $^{1}H_N$ (bottom) R_2 relaxation data for the 60 μM Aβ(1−40) sample recorded at 900 MHz. The solid lines are single-exponential best fits.

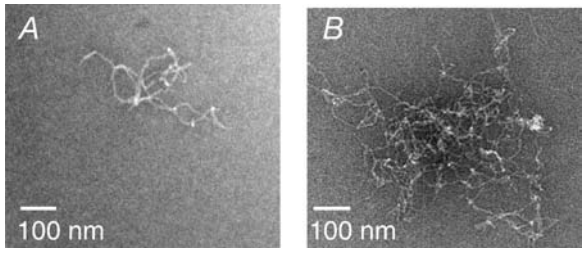

Figure 2. Transmission EM images of negatively stained (A) 150 and (B) 300 μM Aβ(1−40) NMR samples after >3 weeks of equilibration.

The observation that the R_2 rate enhancements as a function of total Aβ(1−40) concentration are independent of nucleus and magnetic field and, in addition, vary only slightly along the peptide indicates that the R_2 rate increases cannot be due to exchange line broadening on the fast/intermediate chemical shift time scale. The latter is dependent on the difference in the resonance frequencies of the spins involved and therefore strongly affected by the nucleus' chemical environment and the external magnetic field used in the measurements.[19] It is also important to stress that the observed resonances arise only from the monomeric Aβ(1−40) peptide and not from any aggregates present. Indeed, intermolecular paramagnetic relaxation enhancement (PRE) measurements, which provide a highly sensitive probe for the presence of low populations of self-associated species in fast (microsecond to millisecond) exchange with monomer,[20a,b] showed no transverse PRE rate enhancements above a reliable detection limit of $\sim 5\ s^{-1}$ for mixtures of ^{15}N-labeled

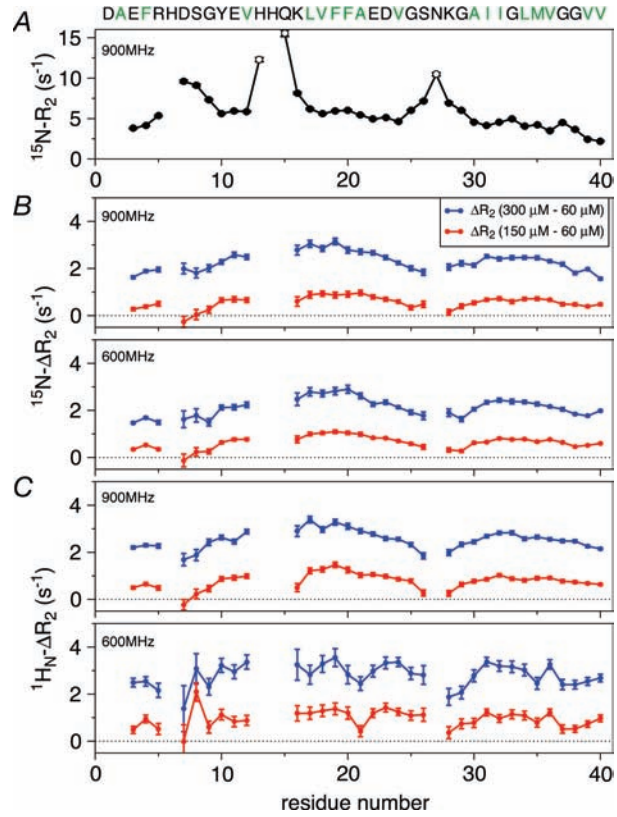

Figure 3. Transverse relaxation rates (R_2) measured on equilibrated samples of Aβ(1−40). (A) ^{15}N R_2 at 900 MHz for 60 μM Aβ(1−40). Cross-peaks for Ala2, His6, and His14 are not sufficiently resolved to permit accurate determination of R_2 rates. The difference in R_2 relaxation rates, ΔR_2, between 300 (blue) or 150 (red) μM samples and the 60 μM sample for (B) ^{15}N (top, 900 MHz; bottom, 600 MHz) and (C) $^{1}H_N$ (top, 900 MHz; bottom, 600 MHz). Large R_2 rates and uncertainties in their values preclude reliable determination of ΔR_2 for His13, Gln15, and Asn27 (A, open circles) and hence are excluded in (B) and (C). The peptide sequence, with hydrophobic residues colored in green, is presented at the top of the figure. (Error bars, 1 SD.)

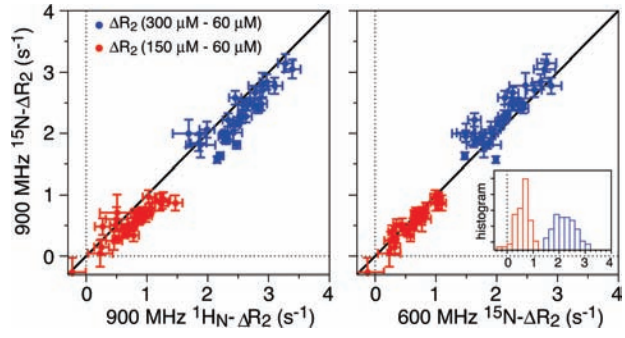

Figure 4. ΔR_2 is independent of nucleus and magnetic field. Correlation plots of ^{15}N-ΔR_2 at 900 MHz vs $^{1}H_N$-ΔR_2 at 900 MHz (left panel) and ^{15}N-ΔR_2 at 600 MHz (right panel). The ΔR_2(300 μM - 60 μM) and ΔR_2(150 μM - 60 μM) rates are colored in blue and red, respectively. A line with slope of unity is displayed for comparison. A histogram of the distribution of ^{15}N-ΔR_2 rates is shown as an inset.

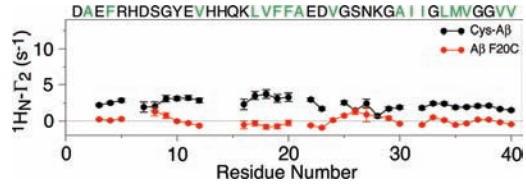

Figure 5. Intermolecular PRE profiles for Aβ(1−40). Transverse ^1H_N PRE rates, ^1H_N Γ_2, were determined from the difference in transverse relaxation rates, ^1H_N R_2, between paramagnetic and diamagnetic samples. The samples comprised 100 μM U-[^{15}N]-labeled Aβ(1−40) and 170 μM single-cysteine variant Aβ(1−40) peptides at natural isotopic abundance conjugated to either a nitroxide spin-label or a diamagnetic analogue. A Cys residue was introduced preceding the N-terminal Asp residue (Cys-Aβ, black) or as an F20C mutation in the center of the peptide (red). For the Cys-Aβ variant, only small, intermolecular PREs (^1H_N Γ_2 < 5 s^{-1}) were observed, while essentially no intermolecular PREs were observed for the F20C sample.

Aβ(1−40) and nitroxide spin-labeled Aβ(1−40) at natural isotopic abundance (Figure 5). Thus, either the population of lower order, transient, self-associated states, if present, is less than 1−2%,[20c] or such exchange is slow on the PRE time scale (<ca. 1 ms). We conclude that the observed R_2 rate enhancements must be due to a lifetime broadening effect arising from direct incorporation of the NMR-visible monomer into NMR-invisible oligomers (i.e., a "dark" state).

The transverse magnetizations of any large oligomeric species will decay very rapidly owing to the very large R_2 rates associated with their high molecular weights. Hence, the observed increase in R_2 rates at high concentration of Aβ(1−40) can be interpreted as the unidirectional monomer-to-oligomer conversion rate under pseudo-equilibrium conditions. The maximum observed ^{15}N ΔR_2 rates of 1.1 and 3.1 s^{-1} at total Aβ(1−40) concentrations of 150 and 300 μM, respectively, provide estimates of the apparent first-order association rate constants, k_{on}^{app}, for this process. A similar phenomenon has been observed for the equilibrium between monomeric and lipid-bound α-synuclein.[21]

To probe the invisible oligomeric state, we carried out a series of ^{1}H saturation transfer experiments. Using 1 s off-resonance continuous wave (CW) pulses with radiofrequency (RF) field strengths of 180 or 350 Hz at a series of offsets (ranging from +35 to −35 kHz) from the water resonance, the underlying broad resonances of the large oligomers were partially saturated, and transfer of saturation from the "dark" oligomeric states to the monomer was measured from the overall decrease in intensity of the ^1H_N backbone amide envelope (7.8−9 ppm) of the monomer in a one-dimensional ^{1}H NMR spectrum relative to that in a reference spectrum obtained without saturation.

For the 60 μM Aβ(1−40) sample, the off-resonance saturation pulse has no effect on the signal intensity of the amide resonances until the saturation pulse approaches resonances of the protein (Figure 6, black), as expected for a monomeric peptide or protein. For the 300 μM Aβ(1−40) sample, however, the amide resonances are uniformly attenuated by the CW pulse at RF offsets far off-resonance (Figure 6, orange and blue), due to transfer of saturation from the invisible "dark" state with large R_2.

Exchange between free monomer (M_{free}) and transiently bound monomer (M_{bound}) in the NMR-invisible "dark" state can be represented phenomenologically by a pseudo-first-order process (see Supporting Information):

$$M_{free} \underset{k_{off}}{\overset{k_{on}^{app}}{\rightleftharpoons}} M_{bound} \qquad (1)$$

The values of the dissociation rate constant, k_{off}, and the R_2^{dark} rate for the "dark" state can be obtained by simultaneously fitting the

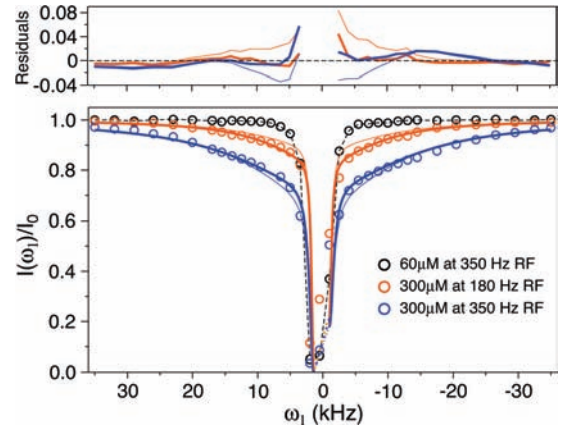

Figure 6. Attenuation of the integrated intensity of the ^1H_N envelope of monomeric Aβ(1−40) by transfer of saturation from the "dark" state following application of an off-resonance radio frequency (RF) field as a function of offset from the water resonance. Black circles, 60 μM total concentration and 350 Hz RF field; orange and blue circles, 300 μM total concentration with 180 and 350 Hz RF fields, respectively. The simultaneous best-fits to the experimental saturation profiles for the 300 μM sample at the two RF fields, using the McConnell equations for a dipolar-coupled two-spin, two-site exchange model, are significantly better with two distinct R_2^{dark} rates (bold orange and blue lines) than with a single R_2^{dark} rate (thin orange and blue lines). Dotted blue and orange lines indicate the region near-resonance where saturation is not well represented by the model due to the many-spin nature of the experimental system. Plots of the residuals (observed minus calculated) between the experimental saturation profiles and the best-fit curves are shown in the top panel. The model with the single R_2^{dark} underestimates the attenuation between 5 kHz < |RF offset| < 20 kHz at the lower (180 Hz) RF field while overestimating the attenuation between −15 kHz < RF offset < −5 kHz and between +5 kHz < RF offset < +10 kHz at the higher (350 Hz) RF field. The best-fit parameters for the model with a single R_2^{dark} rate are R_2^{dark} = 66 000 ± 9000 s^{-1} and k_{off} = 320 ± 20 s^{-1}. The best-fit parameters for the model with two R_2^{dark} rates are k_{off} = 73 ± 6 s^{-1}, R_2^{dark}(large) = 42 000 ± 3000 s^{-1}, and R_2^{dark}(small) ≤ 300 s^{-1} with population weights of 0.40 ± 0.03 and 0.60 ± 0.03, respectively.

experimental saturation profiles for the 300 μM sample at the two RF field strengths to a solution of the McConnell equations[22] for two dipolar-coupled spins in two-site exchange in the presence of a CW saturation field (see Supporting Information). Inclusion of two dipolar-coupled spins with different resonance frequencies was necessary to account for the ∼5 kHz width of the saturation profile observed for the 60 μM sample (black circles in Figure 6), where the fraction of oligomers is negligible (Figure 1B): the width of the saturation profile spans the ^{1}H chemical shift range of the monomer and is ascribed to saturation transfer arising from cross-relaxation among protons in the monomer.

Given measured values of ^1H_N R_1 = 1 s^{-1} and ^1H_N R_2 = 10 s^{-1} for the Aβ(1−40) monomer, k_{on}^{app} = 3.1 s^{-1}, and assuming the cross-relaxation rates are small in the monomer (−0.5 to −3 s^{-1}) but large in the oligomer (∼ −500 s^{-1}), the saturation profiles for the 300 μM sample can be fit with k_{off} = 73 ± 6 s^{-1} and two distinct values of R_2^{dark}: 42 000 ± 3000 s^{-1} and ∼300 s^{-1} with weights of 0.40 ± 0.03 and 0.60 ± 0.03, respectively (Figure 6, thick orange and blue lines). The saturation profiles for the 300 μM sample cannot be adequately fit by a model with only a single R_2^{dark} rate (Figure 6, thin orange and blue lines) but are not inconsistent with a distribution of larger and smaller R_2^{dark} rates.

If R_2^{dark} varies along the peptide chain, ranging from ∼300 to ∼40 000 s^{-1}, the residues with the largest R_2^{dark} rates would have broad saturation profiles, while those with smaller R_2^{dark} rates would experience saturation profiles close to that of the free monomer. Because only a small fraction of monomer is involved in transient interactions with the oligomer ($k_{off} \gg k_{on}^{app}$), ^1H_N resonances with

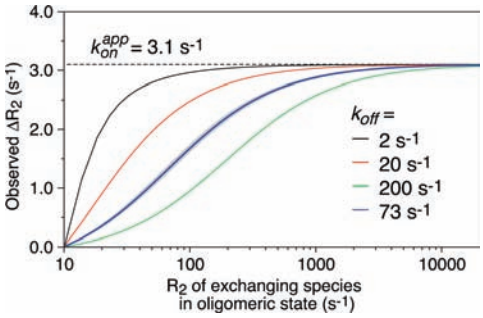

Figure 7. Simulation of the dependence of the monomer ΔR_2 rates arising from exchange with an NMR-invisible, oligomer-bound species as a function of the R_2 rate in the bound state obtained by numerical solution of the McConnell equations. The blue curve is calculated using the experimentally determined values of 3.1 and 73 s^{-1} for k_{on}^{app} and k_{off}, respectively, obtained for the 300 μM Aβ(1−40) sample. The ΔR_2 predicted for $k_{off} \pm 6$ s^{-1} (the 68% confidence interval, representing ± 1 SD) is represented by the gray region. Calculated ΔR_2 rates as a function of the R_2 rate in the oligomeric state for k_{off} values of 2 (black), 20 (red), and 200 (green) s^{-1} are also shown for comparison. The effect of ^{1}H chemical shift differences between free and oligomer-bound monomers on the observed ΔR_2 is assumed to be negligible. Residue positions tightly interacting with the oligomer, such as the central hydrophobic region, may have large chemical shift deviations upon binding, but these effects are far exceeded by the large R_2 (ca. 40 000 s^{-1}) at those positions, which causes complete decay of transverse magnetization of these residues in the oligomer-bound monomer. In contrast, residue positions retaining significant mobility in the oligomer-bound form have much lower R_2 values (ca. 300 s^{-1}); hence, their chemical shift changes are likely to be small since the average environment of these highly disordered residues is likely to be very similar to that in the unstructured free state. Further, the ^{15}N CPMG R_2 experiment, with a 180° pulse separation time of 900 μs, should suppress the effects arising from chemical exchange for moderate shift differences (<200 Hz). The correspondence of the ΔR_2 measured on two different nuclei (^1H_N and ^{15}N R_2 relaxation) at two different fields (600 and 900 MHz) (Figure 3) further supports this assumption of negligible effects of shift differences upon chemical exchange.

smaller R_2^{dark} rates will make a negligible contribution to a standard 1D ^{1}H NMR spectrum such that only signals of the free monomer are observed. Further, because k_{off} is large, the lifetime broadening effect (ΔR_2) will be smaller in the case of residues having smaller R_2^{dark} rates (Figure 7), thereby explaining the small variation in ΔR_2 as a function of residue (Figure 3). Thus, the lower observed ΔR_2 rates for the first nine N-terminal residues (which are disordered in Aβ fibrils[7,23]), as well as for residues 24−29 (which form a turn between the two hydrophobic segments in Aβ fibrils[7a,23]), can be attributed to their higher mobility in the oligomer-bound state. Regions in intimate contact with the oligomer exhibit maximal ΔR_2 rates equal to the unidirectional on-rate k_{on}^{app}, as exemplified by the central hydrophobic region. The optimized weights of 40 and 60% for the large and small R_2^{dark} rates obtained from the fits to the saturation profiles (Figure 6) are fully consistent with the number of residues exhibiting larger and smaller ΔR_2 values, respectively (Figures 3 and 4).

The fraction, f_{ex}, of peptide within the oligomeric "dark" state that exchanges with free monomer is given by the ratio of $[M_{bound}]$ to total peptide sample concentration. f_{ex} is readily calculated from the values of k_{off}, k_{on}^{app}, and $[M_{free}]$ and found to be 3.5 and 3.3% for the 150 and 300 μM Aβ(1−40) samples, respectively, indicating that the data at the two sample concentrations are self-consistent. Thus, only 1 in about 30 peptides within the oligomer undergoes exchange with free monomer, suggesting that exchange occurs predominantly from the ends of the oligomers.

In conclusion, we have demonstrated that large oligomers of the Aβ(1−40) peptide are in dynamic equilibrium with the monomeric state on a time scale of 10−15 ms, and that monomers are constantly binding and being released from NMR-invisible oligomers. This process is slower than the fast transient (microsecond to millisecond time scale) self-association of monomers that gives rise to sizable intermolecular PREs observed for α-synuclein.[24] The small regional specificity for ΔR_2 indicates that the N-terminal nine residues remain highly mobile, while the central and C-terminal hydrophobic regions are largely immobilized upon association of monomer onto the surface of the oligomeric species. Rapid exchange between monomeric and polymorphous oligomeric forms suggests that therapeutic efforts aimed at altering the equilibrium between these species may be more successful than for extremely stable amyloid fibrils.

Acknowledgment. We thank M. Doucleff for help with the early part of this work; A. Szabo, A. Bax, R. Tycko, C. Bewley, D. Baber, and D. Garrett for discussions. This work was supported by the intramural program of NIDDK and the AIDS Targeted Antiviral Program of the NIH Director (to G.M.C.).

Supporting Information Available: ^{15}N and ^1H_N R_2 values, supplementary methods, and complete ref 10c. This material is available free of charge via the Internet at http://pubs.acs.org.

References

(1) Goedert, M.; Spillantini, M. G. *Science* **2006**, *314*, 777–781.
(2) Querfurth, H. W.; LaFerla, F. M. *New Engl. J. Med.* **2010**, *362*, 329–344.
(3) Walsh, D. M.; Selkoe, D. J. *J. Neurochem.* **2007**, *101*, 1172–1184.
(4) Fukumoto, H.; Tokuda, T.; Kasai, T.; Ishigami, N.; Hidaka, H.; Kondo, M.; Allsop, D.; Nakagawa, M. *FASEB J.* **2010**; 0:fj.09-150359v1 epub.
(5) Pimplikar, S. W. *Int. J. Biochem. Cell Biol. J* **2009**, *41*, 1261–1268.
(6) Serpell, L. C.; Fraser, P. E.; Sunde, M. *Methods Enzymol.* **1999**, *309*, 526–536.
(7) (a) Paravastu, A. K.; Qahwash, I.; Leapman, R. D.; Meredith, S. C.; Tycko, R. *Proc. Natl. Acad. Sci. U.S.A.* **2009**, *106*, 7443–7448. (b) Petkova, A. T.; Ishii, Y.; Balbach, J. J.; Antzutkin, O. N.; Leapman, R. D.; Delaglio, F.; Tycko, R. *Proc. Natl. Acad. Sci. U.S.A.* **2002**, *99*, 16742–16747. (c) Petkova, A. T.; Leapman, R. D.; Guo, Z. H.; Yau, W. M.; Mattson, M. P.; Tycko, R. *Science* **2005**, *307*, 262–265.
(8) Chen, B.; Thurber, K. R.; Shewmaker, F.; Wickner, R. B.; Tycko, R. *Proc. Natl. Acad. Sci. U.S.A.* **2009**, *106*, 14339–14344.
(9) Luhrs, T.; Ritter, C.; Adrian, M.; Riek-Loher, D.; Bohrmann, B.; Doeli, H.; Schubert, D.; Riek, R. *Proc. Natl. Acad. Sci. U.S.A.* **2005**, *102*, 17342–17347.
(10) (a) Bernstein, S. L.; Dupuis, N. F.; Lazo, N. D.; Wyttenbach, T.; Condron, M. M.; Bitan, G.; Teplow, D. B.; Shea, J. E.; Ruotolo, B. T.; Robinson, C. V.; Bowers, M. T. *Nature Chem.* **2009**, *1*, 326–331. (b) Rahimi, F.; Shanmugam, A.; Bitan, G. *Curr. Alzheimer Res.* **2008**, *5*, 319–341. (c) Yu, L.; et al. *Biochemistry* **2009**, *48*, 1870–1877.
(11) Teplow, D. B.; Lazo, N. D.; Bitan, G.; Bernstein, S.; Wyttenbach, T.; Bowers, M. T.; Baumketner, A.; Shea, J. E.; Urbanc, B.; Cruz, L.; Borreguero, J.; Stanley, H. E. *Acc. Chem. Res.* **2006**, *39*, 635–45.
(12) (a) Knowles, T. P.; Waudby, C. A.; Devlin, G. L.; Cohen, S. I.; Aguzzi, A.; Vendruscolo, M.; Terentjev, E. M.; Welland, M. E.; Dobson, C. M. *Science* **2009**, *326*, 1533–1537. (b) Bellesia, G.; Shea, J. E. *J. Chem. Phys.* **2009**, *131*, 111102. (v) Lee, C. F.; Loken, J.; Jean, L.; Vaux, D. J. *Phys. Rev. E Stat. Nonlin. Soft Matter Phys.* **2009**, *80*, 041906.
(13) Hou, L. M.; Zagorski, M. G. *J. Am. Chem. Soc.* **2006**, *128*, 9260–9261.
(14) Iwahara, J.; Tang, C.; Clore, G. M. *J. Magn. Reson.* **2007**, *184*, 185–195.
(15) Yan, Y.; Wang, C. *J. Mol. Biol.* **2006**, *364*, 853–862.
(16) Yan, Y.; Wang, C. *J. Mol. Biol.* **2007**, *369*, 909–916.
(17) Almstedt, K.; Nystrom, S.; Nilsson, K. P.; Hammarstrom, P. *Prion* **2009**, *3*, 224–235.
(18) Wang, C. Y.; Grey, M. J.; Palmer, A. G. *J. Biomol. NMR* **2001**, *21*, 361–366.
(19) Mittermaier, A.; Kay, L. E. *Science* **2006**, *312*, 224–228.
(20) (a) Clore, G. M. *Mol. Biophys.* **2008**, *4*, 1058–1069. (b) Tang, C.; Iwahara, J.; Clore, G. M. *Nature* **2006**, *444*, 383–386. (c) Tang, C.; Ghirlando, R.; Clore, G. M. *J. Am. Chem. Soc.* **2008**, *130*, 4048–4056.
(21) Bodner, C. R.; Dobson, C. M.; Bax, A. *J. Mol. Biol.* **2009**, *390*, 775–790.
(22) (a) McConnell, H. M. *J. Chem. Phys.* **1958**, *28*, 430–431. (b) Helgstrand, M.; Hart, T.; Allard, P. *J. Biomol. NMR* **2000**, *18*, 49–63.
(23) Petkova, A. T.; Yau, W. M.; Tycko, R. *Biochemistry* **2006**, *45*, 498–512.
(24) Wu, K. P.; Baum, J. *J. Am. Chem. Soc.* **2010**, *132*, 5546–5547.

JA1048253